

Critical velocity of flowing supersolids of dipolar Bose gases in optical lattices

Ippei Danshita^{1*} and Daisuke Yamamoto²

¹*Department of Physics, Faculty of Science, Tokyo University of Science, Shinjuku-ku, Tokyo 162-8601, Japan*

²*Department of Physics, Waseda University, Shinjuku-ku, Tokyo 169-8555, Japan*

(Dated: October 17, 2018)

We study superfluidity of supersolid phases of dipolar Bose gases in two-dimensional optical lattices. We perform linear stability analyses for the corresponding dipolar Bose-Hubbard model in the hardcore boson limit to show that a supersolid can have stable superflow until the flow velocity reaches a certain critical value. The critical velocity for the supersolid is found to be significantly smaller than that for a conventional superfluid phase. We propose that the critical velocity can be used as a signature to identify the superfluidity of the supersolid phase in experiment.

PACS numbers: 03.75.Hh, 03.75.Lm, 05.30.Jp

I. INTRODUCTION

New possibilities to explore exotic quantum phases have been pioneered by recent experimental advances in creating dipolar ultracold gases [1, 2], such as the realization of a condensate of ⁵²Cr atoms with strong magnetic dipole moments [3, 4] and heteronuclear polar molecules [5, 6]. Thanks to the long-range nature and anisotropy of the dipole-dipole interactions, various quantum phases have been predicted to emerge, including fermionic superfluids (SF) with *p*-wave pairing [2, 7], Haldane-Bose insulators [8], and supersolids (SS) [9–14].

Of particular interest are SS phases, in which both diagonal (crystalline) and off-diagonal (superfluid) long-range orders coexist [15]. Although non-classical rotational inertia, one of the signatures of superfluidity, was experimentally observed in solid helium [16], it has been more reasonably interpreted by other mechanisms, such as superfluidity of grain boundaries and dislocations [17, 18]. On the other hand, quantum Monte Carlo (QMC) simulations have shown the presence of SS phases in Bose-Hubbard systems with long-range interactions [13, 14, 19, 20]. Since QMC analyses of the Bose-Hubbard model quantitatively agree with experiments of ultracold gases in optical lattices, the SS phases are expected to be found in the context of dipolar Bose gases loaded into optical lattices.

In order to verify the existence of SS in experiments of ultracold gases, one has to clarify observables to identify the superfluidity and the crystalline order of the SS phases. It is well-known that the crystalline order can be identified by the static structure factor, which has been observed in cold atom experiments using the Bragg scattering techniques [21, 22]. On the other hand, a sharp interference peak in the time-of-flight image following the expansion of a gas is often used as an indirect indication of the superfluidity of Bose gases in optical lattices [23]. However, the sharp interference peak identifies the presence of a Bose-Einstein condensate, but does not nec-

essarily mean the superfluidity. For instance, although a non-interacting Bose gas forms a condensate at sufficiently low temperature, it is not a SF in the sense that its critical velocity is zero [24]. Moreover, while most previous theoretical work calculated the SF fraction as a characteristic of the superfluidity [13, 14, 19, 20], so far no experiment has succeeded in measuring the SF fraction in cold atom systems [25], in contrast to helium systems where the SF fraction, corresponding to the non-classical rotational inertia, can be easily measured with a torsional oscillator [16, 17]. Instead, the superfluidity of weakly- [27] and strongly-interacting Bose gases [28], and fermionic SF across the BEC-BCS crossover [29] has been demonstrated in a moving optical lattice by measuring the critical velocity above which superflow breaks down.

In this paper, we propose that the superfluidity of SS phases can also be experimentally identified using a moving optical lattice. Performing linear stability analyses for polarized dipolar hardcore bosons in a two-dimensional (2D) moving optical lattice, we show that superflow of SS states is stable until the flow momentum exceeds a certain finite value. It is found that the critical momenta for the dynamical instability in the SS phases are remarkably smaller than that for a standard SF with no density wave order. We argue that the critical momenta can be experimentally measured with currently available techniques.

The remainder of the paper is organized as follows. In Sec. II, we introduce our model Hamiltonian describing hardcore bosons with dipole-dipole interaction in a 2D optical lattice. In Sec. III, we explain our formulation of the problem based on a mean-field theory. In Sec. IV, we calculate the ground-state phase diagram. In Sec. V, we perform linear stability analyses to obtain the critical velocities for Landau and dynamical instabilities in the SF and SS phases. In Sec. VI, we summarize our results and briefly discuss two recent experiments exploring SS phases in cold atom systems [30, 31].

*Present address: RIKEN, Wako, Saitama 351-0198, Japan

II. MODEL

We consider a system of N bosons interacting with on-site and dipole-dipole interactions in a 2D optical lattice. The dipoles are assumed to be polarized to the direction perpendicular to the lattice plane. This system can be well-described by the dipolar Bose-Hubbard model [9],

$$\hat{H} = -J \sum_{\langle j,l \rangle} (\hat{a}_j^\dagger \hat{a}_l + \text{h.c.}) + \frac{U}{2} \sum_j \hat{n}_j (\hat{n}_j - 1) + \sum_{j<l} V_{jl} \hat{n}_j \hat{n}_l - \mu \sum_j \hat{n}_j, \quad (1)$$

where \hat{a}_j^\dagger is the boson creation operator at site j , $\hat{n}_j = \hat{a}_j^\dagger \hat{a}_j$, J is the hopping, and U is the onsite interaction. The chemical potential μ controls the filling factor $n \equiv N/M$, where M is the total number of lattice sites. $\langle j, l \rangle$ represents nearest-neighbor pairs of lattice sites. The long-range part of the dipole-dipole interaction is well-approximated as $V_{jl} = Vd^3 |\mathbf{r}_j - \mathbf{r}_l|^{-3}$, where j_x and j_y are integers and d is the lattice spacing. In experiments, the ratios J/V and U/V can be controlled by varying the lattice depth and using the Feshbach resonance [4].

In the hardcore boson limit ($U \rightarrow \infty$), Eq. (1) can be mapped onto the following spin-1/2 Hamiltonian,

$$\hat{H}_s = -J \sum_{\langle j,l \rangle} (\hat{S}_j^+ \hat{S}_l^- + \text{h.c.}) + \sum_{j<l} V_{jl} \hat{S}_j^z \hat{S}_l^z - h \sum_j \hat{S}_j^z, \quad (2)$$

where the spin operators are related to the operators of the hardcore boson as $\hat{S}_j^- = \hat{a}_j$ and $\hat{S}_j^z = \hat{n}_j - 1/2$. $h = \mu - 2C_+V$ is the shifted chemical potential, where

$$C_{\pm} = \sum_{\alpha=1}^{\infty} \frac{(\pm 1)^{\alpha-1}}{\alpha^3} + \sum_{\alpha_x, \alpha_y=1}^{\infty} \frac{(\pm 1)^{\alpha_x + \alpha_y - 1}}{(\alpha_x^2 + \alpha_y^2)^{3/2}}. \quad (3)$$

These coefficients include the long-range nature of the dipole-dipole interaction and their numerical values are $C_+ \simeq 2.258$ and $C_- \simeq 0.6615$. The dynamics of the spin model Eq. (2) is described by the Heisenberg equation of motion for \hat{S}_j^+ (we set $\hbar = 1$),

$$i \frac{d}{dt} \hat{S}_j^+ = -2J \hat{S}_j^z \sum_{\langle l \rangle} \hat{S}_l^+ - \hat{S}_j^+ \sum_{l \neq j} V_{jl} \hat{S}_l^z + h \hat{S}_j^z, \quad (4)$$

where $\langle l \rangle$ represents the nearest-neighboring sites to site j .

III. MEAN-FIELD THEORY

Our formulation of the problem is based on a mean-field theory, in which a many-body wave function is approximated as a product of the local spin coherent states,

$$|\Phi_{\text{MF}}\rangle = \prod_j \left(e^{-\frac{i\varphi_j}{2}} \cos \frac{\theta_j}{2} |\uparrow\rangle_j + e^{\frac{i\varphi_j}{2}} \sin \frac{\theta_j}{2} |\downarrow\rangle_j \right), \quad (5)$$

where θ_j and φ_j are the elevation and azimuthal angles of the spin direction at site j . Replacing \hat{S}_j^z and \hat{S}_j^+ with $\langle \hat{S}_j^z \rangle = \frac{1}{2} \cos \theta_j$ and $\langle \hat{S}_j^+ \rangle = \frac{1}{2} e^{i\varphi_j} \sin \theta_j$ in Eqs. (2) and (4), we obtain the mean-field energy $\mathcal{H}_0 \equiv \langle \hat{H}_s \rangle$ given by

$$\mathcal{H}_0 = -\frac{J}{2} \sum_{\langle j,l \rangle} \sin \theta_j \sin \theta_l \cos \varphi_{jl} + \frac{1}{4} \sum_{j<l} V_{jl} \cos \theta_j \cos \theta_l - \frac{h}{2} \sum_j \cos \theta_j \quad (6)$$

and the classical equations of motion for θ_j and φ_j :

$$\frac{d\theta_j}{dt} = J \sum_{\langle l \rangle} \sin \theta_l \sin \varphi_{jl}, \quad (7)$$

$$\frac{d\varphi_j}{dt} = J \sum_{\langle l \rangle} \frac{\sin \theta_l \cos \theta_j}{\sin \theta_j} \cos \varphi_{jl} + \frac{1}{2} \sum_{l \neq j} V_{jl} \cos \theta_l - h, \quad (8)$$

where $\varphi_{jl} \equiv \varphi_j - \varphi_l$. Equation (7) is the continuity equation while Eq. (8) corresponds to the Josephson's acceleration equation. The hardcore boson density $n_j \equiv \langle \hat{n}_j \rangle$, the density $n_j^{\text{con}} = |\langle \hat{a}_j \rangle|^2$, and the phase $\phi_j = \arg(\langle \hat{a}_j \rangle)$ of the condensate wave function, and the spin angles are related by $n_j = (\cos \theta_j + 1)/2$, $n_j^{\text{con}} = n_j(1 - n_j)$, and $\phi_j = -\varphi_j$.

Considering small-amplitude oscillations around a steady solution, we write the solution of Eqs. (7) and (8) in the form

$$\theta_j(t) = \bar{\theta}_j + \delta\theta_j e^{-i\omega t}, \quad \varphi_j(t) = \bar{\varphi}_j + \delta\varphi_j e^{-i\omega t}, \quad (9)$$

where ω is the frequency of the normal mode. Substituting Eq. (9) into Eqs. (7) and (8) and neglecting the terms higher than the first order with respect to $\delta\theta_j$ and $\delta\varphi_j$, we obtain the equations for a steady state

$$\sum_{\langle l \rangle} \sin \bar{\theta}_l \sin \bar{\varphi}_{jl} = 0, \quad (10)$$

$$h = J \sum_{\langle l \rangle} \frac{\sin \bar{\theta}_l \cos \bar{\theta}_j}{\sin \bar{\theta}_j} \cos \bar{\varphi}_{jl} + \frac{1}{2} \sum_{l \neq j} V_{jl} \cos \bar{\theta}_l, \quad (11)$$

and the linearized equations for fluctuations

$$\begin{aligned} -i\omega \delta\theta_j &= J \sum_{\langle l \rangle} [\delta\varphi_{jl} \sin \bar{\theta}_l \cos \bar{\varphi}_{jl} + \delta\theta_l \cos \bar{\theta}_l \sin \bar{\varphi}_{jl}], \quad (12) \\ -i\omega \delta\varphi_j &= J \sum_{\langle l \rangle} \left[\left(\delta\theta_l \frac{\cos \bar{\theta}_j \cos \bar{\theta}_l}{\sin \bar{\theta}_j} - \delta\theta_j \frac{\sin \bar{\theta}_l}{\sin^2 \bar{\theta}_j} \right) \cos \varphi_{jl} \right. \\ &\quad \left. - \delta\varphi_{jl} \frac{\cos \bar{\theta}_j \sin \bar{\theta}_l \sin \bar{\varphi}_{jl}}{\sin \bar{\theta}_j} \right] - \frac{1}{2} \sum_{l \neq j} V_{jl} \delta\theta_l \sin \bar{\theta}_l. \quad (13) \end{aligned}$$

The excitation energy ω calculated from Eqs. (12) and (13) coincides with that calculated by linear spin-wave theory [32]. Stability of a steady solution can be discriminated by ω . The appearance of excitations with $\omega < 0$

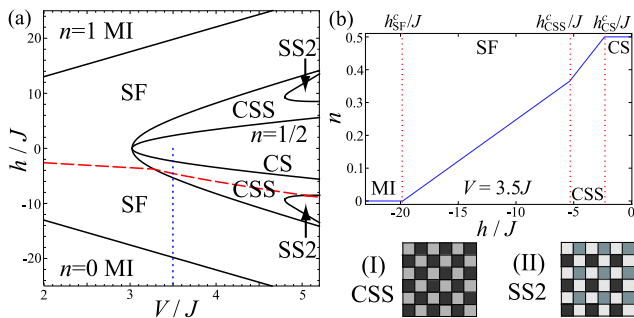


FIG. 1: (color online) (a) Ground-state phase diagram of the hardcore Bose-Hubbard model with the dipole-dipole interaction in the $(V/J, h/J)$ -plane, where MI, SF, CSS, CS, and SS2 phases are present. The dashed red line represents the contour of $n = 0.4$. (b) The filling factor n as a function of h/J . The dotted red lines locate the boundaries between the different phases. The dipolar interaction is fixed to be $V = 3.5J$, which is indicated by the dotted blue line in (a). (I) and (II) Schematic pictures of the CSS and SS2 phases.

signals the Landau instability (LI), while the appearance of excitations with $\text{Im}[\omega] \neq 0$ signals the dynamical instability (DI), which means exponential growth of the fluctuations in time. The linear stability analyses on the basis of Eqs. (12) and (13) allow us to calculate the critical velocity of superflow.

Previous theoretical analyses have shown that the mean-field theory fails to describe even qualitatively the ground-state phase diagram of the hardcore Bose-Hubbard model with nearest- and next-nearest-neighbor interactions due to strong quantum fluctuations [20, 32]. More specifically, while the mean-field theory predicts the presence of a stable checkerboard supersolid (CSS) phase [32], this SS phase is unstable towards phase separation according to accurate QMC simulations. However, the mean-field theory is qualitatively valid for our dipolar hardcore Bose-Hubbard model of Eq. (2), because the long-range nature of the dipolar interaction significantly suppresses quantum fluctuations [33]. We will indeed show in the next section that the mean-field phase diagram for Eq. (2) qualitatively agrees with the recent QMC results of Ref. [13]. We do not argue that the mean-field theory can provide *quantitatively* correct results, but that it is useful for gaining qualitative features and analytical insights of the critical velocity. Notice that so far the QMC methods have not succeeded in calculating the critical velocity.

IV. PHASE DIAGRAM FOR $K = 0$

Within the mean-field theory, let us first calculate the ground-state phase diagram of Eq. (2) in the case that the system does not have a supercurrent, i.e. $\bar{\varphi}_j$ is constant. Without loss of generality, we can consider the spins ordered in the XZ plane ($\bar{\varphi}_j = 0$). To obtain analytical expressions of phase boundaries, we as-

sume that the stationary solution satisfies $\bar{\theta}_j = \theta_{A(B)}$ for $j_x + j_y \in \text{even(odd)}$ [32, 34]. Under this two-sublattice ansatz, we can describe checkerboard solid (CS), SF, CSS, and Mott insulator (MI) phases. The CS phase, termed as the Néel state in the language of the spin model, is an incompressible insulating phase at half filling with a density wave order whose ordering vector is $\mathbf{k}_\pi = (\pi/d, \pi/d)$. This phase is favored in the region of $J, |h| \ll V$, where the antiferromagnetic Ising term is dominant in Eq. (2). The SF phase is characterized by uniform density and finite condensate fraction, i.e. $n_j = n$ and $n_j^{\text{con}} \neq 0$. The latter condition reflects the existence of the off-diagonal long-range order. This phase corresponds to a canted ferromagnetic state in the spin system and is favored when J/V is large or $|h|/V$ is moderately large. The CSS phase possesses both the SF and checkerboard density-wave orders. Recent quantum Monte-Carlo simulations of Eq. (2) in Ref. [13] have shown that the CSS phase is indeed present in the intermediate region between the SF and CS phases. MI is an incompressible phase with $n = 0$ or 1, which corresponds in the spin language to a fully polarized magnetic phase in a strong magnetic field $|h|$. In terms of the spin angle, the conditions for the different phases to emerge is as follows:

$$\begin{aligned} \cos \theta_A = -\cos \theta_B = 1, & \text{ CS,} \\ \theta_A = \theta_B \text{ and } \sin \theta_A \neq 0, & \text{ SF,} \\ \theta_A \neq \theta_B \text{ and } \sin \theta_A \neq 0 \text{ and } \sin \theta_B \neq 0, & \text{ CSS,} \\ \cos \theta_A = \cos \theta_B = \pm 1, & \text{ MI.} \end{aligned} \quad (14)$$

Minimizing the mean-field energy,

$$\begin{aligned} \frac{\mathcal{H}_0}{M} = & -J \sin \theta_A \sin \theta_B + \frac{V}{4}(C_+ + C_-) \cos \theta_A \cos \theta_B \\ & + \frac{V}{8}(C_+ - C_-)(\cos^2 \theta_A + \cos^2 \theta_B) \\ & - \frac{h}{4}(\cos \theta_A + \cos \theta_B), \end{aligned} \quad (15)$$

with respect to θ_A and θ_B , we obtain the phase diagram in the $(V/J, h/J)$ -plane as shown in Fig. 1(a). Reflecting the particle-hole symmetry of the hardcore Bose-Hubbard model, the phase diagram is symmetric with respect to the line $h = 0$.

In Fig. 1(a), it is seen that the CSS and CS phases are present when $V/J > 2/C_-$. Increasing h/J from the $n = 0$ MI region with a fixed value of $V/J > 2/C_-$, the system exhibits the continuous transitions to SF at $h = h_{\text{SF}}^c$, CSS at $h = h_{\text{CSS}}^c$, and CS at $h = h_{\text{CS}}^c$ in order. This behavior is clearly illustrated in Fig. 1(b), where the filling factor n is plotted as a function of h/J . The critical values of h for these transitions are given by

$$\begin{aligned} h_{\text{SF}}^c &= \pm(4J + 2C_+V), \\ h_{\text{CSS}}^c &= \pm 2(C_+V + 2J) \sqrt{\frac{C_-V - 2J}{C_-V + 2J}}, \\ h_{\text{CS}}^c &= \pm 2\sqrt{(C_-V)^2 - 4J^2}. \end{aligned} \quad (16)$$

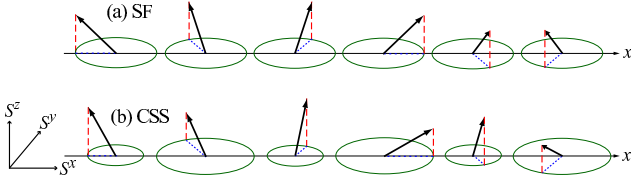


FIG. 2: (color online) Schematic pictures of the SF and CSS states with superflow in the spin representation. The arrows represent the local direction of the spins. The radius of the circles denotes the projection of the spins onto the xy -plane, which corresponds to the local condensate density n_j^{con} . The red dashed lines denote the projection onto the z -axis corresponding to the local density n_j .

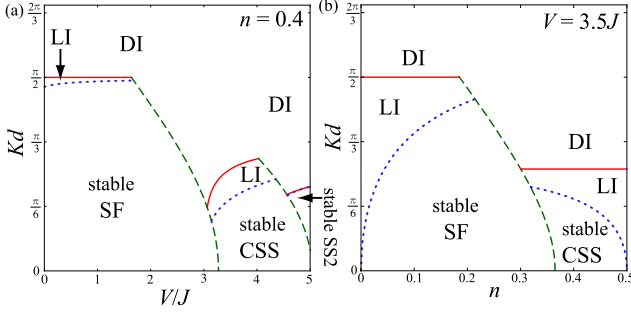


FIG. 3: (color online) Stability phase diagrams of hardcore bosons flowing in a 2D lattice with quasi-momentum $\mathbf{K} = (K, 0)$. In (a) the regions of stable SF, stable CSS, stable SS2, Landau instability (LI), and dynamical instability (DI) are located when V/J is varied for $n = 0.4$, while in (b) those are located when the filling factor n is varied for $V = 3.5J$. The dotted blue, solid red, and dashed green lines represent the critical quasi-momenta for LI, DI caused by phonons, and DI caused by roton-like excitations.

We note that replacing $C_{\pm}V$ with $2(V_1 \pm V_2)$, Eq. (16) coincides with the critical values of h obtained in previous work for the hardcore Bose-Hubbard model with the nearest-neighbor interaction V_1 and the next-nearest-neighbor interaction V_2 [32, 35]. When V/J is increased further, there emerge different solid and SS phases in addition to the phases described above. For instance, allowing for the four-sublattice density modulation, we calcu-

late the boundary to the SS2 phase as shown in Fig. 1(a). The SS2 phase is sketched in Fig. 1(II). We do not push our calculations into the region of $V > 5.2J$, where other solid and SS phases are present, because our purpose is to investigate superfluidity of the SF and CSS phases. Notice that there also exist numerous meta-stable states in the region of large V/J [36], which make experimental investigation of the ground-state phase diagram practically very difficult.

V. EXCITATION SPECTRA AND CRITICAL VELOCITY

Having established the location of the SF and CSS phases in the phase diagram, we next study stability of superflow in these phases by means of a linear stability analysis. Let us consider that the optical lattice confining hardcore bosons is moving at a constant velocity \mathbf{v} . In the coordinate system where the lattice is at rest, the SF component of the hardcore bosons is flowing with quasi-momentum $\mathbf{K} = -m\mathbf{v}$ [27, 28], where m is the particle mass.

In the SF phase, a current-carrying solution of Eqs. (10) and (11) is given by $\bar{\theta}_j = \theta_0$ and $\bar{\varphi}_j = -\mathbf{K} \cdot \mathbf{r}_j$, where θ_0 is related to the filling factor as $\cos \theta_0 = 2n - 1$. This state is sketched in Fig. 2(a). The current carried by this state is given by $\mathbf{j} = 2n(1 - n)J \sum_{m=x,y} \mathbf{e}_m \sin(K_m d)$, where $(K_x, K_y) \equiv \mathbf{K}$, and \mathbf{e}_x and \mathbf{e}_y represent the unit vectors in the x and y directions. Inserting this solution into Eqs. (6) and (11), we obtain the energy per particle $\epsilon_{\mathbf{K}} \equiv (\mathcal{H}_0 + h \sum_j \langle S_j^z \rangle) / N$ and the chemical potential $h_{\mathbf{K}}$ as functions of \mathbf{K} :

$$\epsilon_{\mathbf{K}} = -4(1-n)J\gamma_{\mathbf{K}} + \frac{(1-2n)^2}{2n}C_+V, \quad (17)$$

$$h_{\mathbf{K}} = 2(2n-1)(2J\gamma_{\mathbf{K}} + C_+V). \quad (18)$$

where $\gamma_{\mathbf{K}} = \sum_{m=x,y} \cos(K_m d)/2$. Notice that $\epsilon_{\mathbf{K}}$ and $h_{\mathbf{K}}$ satisfy the thermodynamic relation, $h_{\mathbf{K}} = \frac{\partial(N\epsilon_{\mathbf{K}})}{\partial N}$.

Solving Eqs. (12) and (13), we obtain the excitation spectrum,

$$\omega_{\mathbf{K}}(\mathbf{q}) = (2-4n)J(\gamma_{\mathbf{q}-\mathbf{K}} - \gamma_{\mathbf{q}+\mathbf{K}}) + [4J(2\gamma_{\mathbf{K}} - \gamma_{\mathbf{q}+\mathbf{K}} - \gamma_{\mathbf{q}-\mathbf{K}})\{2J\gamma_{\mathbf{K}} - (1-2n)^2J(\gamma_{\mathbf{q}+\mathbf{K}} + \gamma_{\mathbf{q}-\mathbf{K}}) + n(1-n)V(\mathbf{q})\}]^{\frac{1}{2}}, \quad (19)$$

where \mathbf{q} is the quasi-momentum of the excitation and $V(\mathbf{q})/V = \sum_{\alpha=1}^{\infty} \frac{2}{\alpha^3} \{\cos(\alpha q_x d) + \cos(\alpha q_y d)\} + \sum_{\alpha_x, \alpha_y=1}^{\infty} \frac{4}{(\alpha_x^2 + \alpha_y^2)^{3/2}} \cos(\alpha_x q_x d) \cos(\alpha_y q_y d)$. Stability of superflow in the SF state can be judged by Eq. (19). We assume that the current is flowing in the x -direction, i.e. $\mathbf{K} = (K, 0)$, and depict the stability phase diagrams

in the (n, Kd) - and $(V/J, Kd)$ -planes in Fig. 3. Stability of the hardcore boson system deep in the SF region, e.g. $V \lesssim J$ or $0 < n \ll 0.5$, is analogous to that of softcore boson systems described by the GP mean-field theory [37, 38] in the following way. With increasing K , excitations with $\omega_{\mathbf{K}}(\mathbf{q}) < 0$ appear at a certain value of

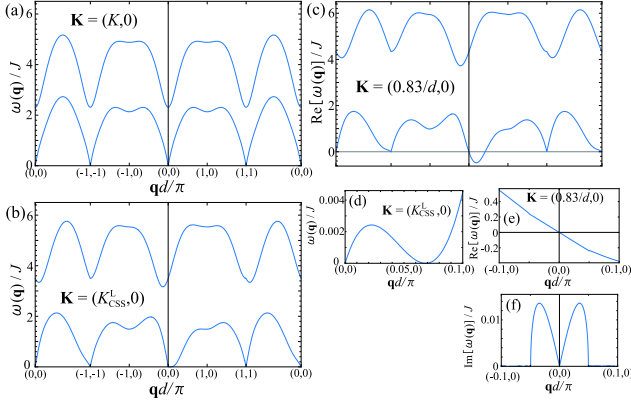


FIG. 4: (color online) Excitation spectra $\omega(\mathbf{q})$ in the CSS phase for $V = 3.5J$, $n = 0.4$, and different values of K in the x -direction, where $K = 0$ (a), $K = K_{CSS}^L$ (b), and $K = 0.83/d > K_{CSS}^D$ (c). (d) and (e) are magnification of (b) and (c) focused on the region of $|q_x| \ll 1/d$ and $q_y = 0$, where excitations with negative and complex energies arise. In (f), the imaginary part of $\omega(\mathbf{q})$ corresponding to (e) is shown.

the quasi-momentum, $K = K_{SF}^L$, signaling LI. In Fig. 3, K_{SF}^L is plotted by the dotted blue line separating the stable SF and LI regions. When $K > K_{SF}^D = \pi/(2d)$, long-wavelength phonons cause DI. This DI reflects the fact that the effective mass in the x -direction, defined by $(\tilde{m}_{\mathbf{K}}^x)^{-1} = \frac{\partial^2 \epsilon_{\mathbf{K}}}{\partial K_x^2}$, is negative, resulting in the imaginary sound speed in the x direction $c_{\mathbf{K}}^x = (\kappa_{\mathbf{K}} \tilde{m}_{\mathbf{K}}^x)^{-1/2}$. Here, $\kappa_{\mathbf{K}}$ is the compressibility.

In the SF region close to the boundary with the CSS phase, the excitation spectrum $\omega_{\mathbf{K}}(\mathbf{q})$ has a roton-like minimum at $\mathbf{q} = \mathbf{k}_{\pi}$ [32]. When K increases in this region, the roton-like excitations cause DI, which signals the transition to the CSS phase [39–42], before LI occurs. The critical value of K for this DI is plotted by the dashed-dotted green line in Fig. 3. Previous theoretical work for the system of hardcore bosons with only nearest-neighbor interaction has predicted that superflow can be destabilized by the roton-like excitations, but that the resulting CSS state with superflow is dynamically unstable [40, 41]. In contrast, we will show below that the flowing CSS state can be stable in our system of dipolar hardcore bosons.

In the CSS phase, solving Eqs. (10) and (11) within the two-sublattice ansatz, we obtain a current-carrying solution,

$$\begin{aligned} \bar{\varphi}_j &= -\mathbf{K} \cdot \mathbf{r}_j, \cos \theta_A = 4n - 2 - \cos \theta_B, \\ \cos \theta_B &= 2n - 1 \pm 2\sqrt{n^2 - n + \frac{1}{2} - \frac{|1 - 2n|C_- V}{2\beta_{\mathbf{K}}}}, \end{aligned} \quad (20)$$

where $\beta_{\mathbf{K}} = \sqrt{(C_- V)^2 - (2J\gamma_{\mathbf{K}})^2}$. A schematic picture of this state is depicted in Fig. 2(b). This state possesses the current $\mathbf{j} = 2|1 - 2n|J^2\gamma_{\mathbf{K}}\beta_{\mathbf{K}}^{-1} \sum_{m=x,y} \mathbf{e}_m \sin(K_m d)$. Substituting Eq. (20) into Eqs. (6) and (11), we obtain

the energy per particle and the chemical potential,

$$\epsilon_{\mathbf{K}} = \frac{|1 - 2n|}{n} \beta_{\mathbf{K}} + \frac{(1 - 2n)^2(C_+ - C_-) - C_-}{2n} V, \quad (21)$$

$$h_{\mathbf{K}} = \text{sgn}(2n - 1) \times 2\beta_{\mathbf{K}} - 2(1 - 2n)(C_+ - C_-)V. \quad (22)$$

In Fig. 4, assuming $\mathbf{K} = (K, 0)$ again, we show the excitation spectra for $V = 3.5J$, $n = 0.4$, and the different values of K . There are two branches of excitation spectrum: one is a gapless and linear mode at low momenta, denoted by $\omega_{\mathbf{K}}^-(\mathbf{q})$, and the other is a gapful mode, denoted by $\omega_{\mathbf{K}}^+(\mathbf{q})$. Since $\omega_{\mathbf{K}}^{\pm}(\mathbf{q}) \geq 0$ until K exceeds a certain critical value, in the stability phase diagrams of Fig. 3 there is a region where the CSS state with finite superflow is stable. Like in the SF phase, we find two scenarios regarding the instability of superflow in the CSS phase. First, sufficiently away from the boundary to the SS2 phase, $\omega_{\mathbf{K}}^-(\mathbf{q})$ is pushed down with increasing K , and it reaches zero at $K = K_{CSS}^L$ (see Figs. 4(b) and (d)), signaling LI. In Fig. 3, K_{CSS}^L is plotted by the dotted blue lines separating the LI and stable CSS regions. When K is increased further, DI caused by phonons at low momenta sets in at $K = K_{CSS}^D$ as seen in Figs. 4(c), (e), and (f). K_{CSS}^D can be determined by the condition $\tilde{m}_{\mathbf{K}}^x = 0$, which is reduced to

$$(C_- V)^2 (2 \cos(Kd) - 1) = J^2 (1 + \cos(Kd))^2 \cos(Kd) \quad (23)$$

When $C_- V \gg J$, we obtain

$$K_{CSS}^D d \simeq \frac{\pi}{3} - \frac{3\sqrt{3}}{8} \frac{J^2}{(C_- V)^2}. \quad (24)$$

In Fig. 3, the right solid red lines represent K_{CSS}^D . It is obvious from Eq. (23) and Fig. 3 that K_{CSS}^D is independent on n and monotonically increases with V/J . It is also worth stressing that K_{CSS}^D is distinctively smaller than K_{SF}^D . We attribute this reduction of the critical quasi-momenta to the difference between the energy band structures in the SF and CSS phases, which are respectively given by Eqs. (17) and (21).

Secondly, near the boundary to the SS2 phase, DI caused by the excitations at $\mathbf{q} = (\pi/d, 0)$ precedes the other instabilities and signals the transition to the SS2 phase. The critical value of K for this DI is plotted by the dashed green line in Fig. 3(a). To complete the stability phase diagram, we also carry out stability analyses for the SS2 state with superflow and locate the stable, LI, and DI regions. Notice that the LI region is almost invisible in Fig. 3(a) because the critical quasi-momentum for LI is nearly equal to that for DI.

Finally, we discuss the feasibility of measuring experimentally the critical quasi-momenta. Experiments of ultracold dipolar Bose gases confined in a moving optical lattice will be performed in an additional parabolic trap. Since the density vanishes at the edge of the trapped gas, the critical quasi-momentum for LI is zero. Hence, for observing superflow, the temperature has to be so low

that the thermal component is invisible and LI cannot destabilize the system [27, 43, 44]. Another consequence of the parabolic trap is that the CSS phase inevitably coexists with other phases if it is present in the trap. For instance, when $n_j = 0.4$ at the trap center and $V = 3.5J$, the CSS phase occupies the central region of the trap and is surrounded by the SF phase. We recall that the critical quasi-momentum $K_{\text{CSS}}^{\text{D}}$ for the DI in CSS is smaller than that in SF and independent on the density. This means that even in the trapped CSS phase coexisting with the SF phase, one can observe dissipationless flow by moving the optical lattice with a velocity smaller than $K_{\text{CSS}}^{\text{D}}/m$ and the breakdown of the superflow when $K_{\text{CSS}}^{\text{D}}/m$ is exceeded. Thus, given that the central density and V/J are precisely controllable in experiments, the stability phase diagrams of Fig. 3 can be investigated in current experimental setups.

VI. SUMMARY

In conclusion, we have studied stability of superflow of dipolar Bose gases in a moving optical lattice. Specifically focusing on the superfluid (SF) and checkerboard supersolid (CSS) phases, we have calculated the critical quasi-momenta for Landau and dynamical instabilities. Superflow in the CSS phases has been found to be stable until the quasi-momentum exceeds the critical value, which is significantly smaller than that in the SF phase. In the CSS phase, we also found the dynamical instability caused by roton-like excitations that results in the transition to another type of supersolid. We emphasize that measuring the critical quasi-momenta will be a di-

rect signature of superfluidity of the SS phases.

Let us make brief comments on two recent experiments [30, 31] that have explored supersolid phases in different contexts from dipolar bosons in optical lattices. One of them has studied spin textures in spin-1 Bose-Einstein condensates (BEC) of ^{87}Rb atoms with the ferromagnetic contact interaction and the dipole-dipole interaction [30]. It was found that the spinor condensate has spatial magnetic order. However, this experiment is not convincing enough to proclaim the discovery of a supersolid phase not only because the magnetic order is short-ranged, but also because the equilibration time of the system is so long that one can not judge whether the magnetically ordered state is really an equilibrium state. The other experiment of Ref. [31] has studied the system of a BEC coupled with an optical cavity and observed the formation of checkerboard density wave order in the BEC associated with the superradiant phase transition. Since the superfluidity of this possible supersolid phase has not been confirmed yet, it will be important to investigate the critical velocity in this system both theoretically and experimentally.

Note added: After the submission of the present paper, there appeared relevant work by Kunimi *et al.*, which studies the critical velocity of a supersolid phase through a single barrier potential [45].

Acknowledgments

We thank Y. Kato for useful comments. The authors are supported by a Grant-in-Aid from JSPS.

-
- [1] T. Lahaye, C. Menotti, L. Santos, M. Lewenstein, and T. Pfau, Rep. Prog. Phys. **72**, 126401 (2009).
 - [2] M. A. Baranov, Phys. Rep. **464**, 71 (2008).
 - [3] A. Griesmaier, J. Werner, S. Hensler, J. Stuhler, and T. Pfau, Phys. Rev. Lett. **94**, 160401 (2005).
 - [4] T. Lahaye, T. Koch, B. Froehlich, M. Fattori, J. Metz, A. Griesmaier, S. Giovanazzi, and T. Pfau, Nature (London) **448**, 672 (2007).
 - [5] K.-K. Ni, S. Ospelkaus, M. H. G. de Miranda, A. Pe'er, B. Neyenhuis, J. J. Zirbel, S. Kotochigova, P. S. Julienne, D. S. Jin, and J. Ye, Science **322**, 231 (2008).
 - [6] S. Ospelkaus, K.-K. Ni, M. H. G. de Miranda, A. Pe'er, B. Neyenhuis, D. Wang, S. Kotochigova, P. S. Julienne, D. S. Jin, and J. Ye, Faraday, Discuss. **142**, 351 (2009).
 - [7] G. M. Bruun and E. Taylor, Phys. Rev. Lett. **101**, 245301 (2008).
 - [8] E. G. Dalla Torre, E. Berg, and E. Altman, Phys. Rev. Lett. **97**, 260401 (2006).
 - [9] K. Goral, L. Santos, and M. Lewenstein, Phys. Rev. Lett. **88**, 170406 (2002).
 - [10] D. L. Kovrizhin, C. V. Pai, and S. Sinha, Europhys. Lett. **72**, 162 (2005).
 - [11] S. Yi, T. Li, and C. P. Sun, Phys. Rev. Lett. **98**, 260405 (2007).
 - [12] I. Danshita and C. A. R. Sá de Melo, Phys. Rev. Lett. **103**, 225301 (2009).
 - [13] B. Capogrosso-Sansone, C. Trefzger, M. Lewenstein, P. Zoller, and G. Pupillo, Phys. Rev. Lett. **104**, 125301 (2010).
 - [14] L. Pollet, J. D. Picon, H. P. Büchler, and M. Troyer, Phys. Rev. Lett. **104**, 125302 (2010).
 - [15] A. F. Andreev and L. M. Lifshitz, Sov. Phys. JETP **29**, 1107 (1969); C. V. Chester, Phys. Rev. A **2**, 256 (1970); A. J. Leggett, Phys. Rev. Lett. **25**, 1543 (1970).
 - [16] E. Kim and M. H. W. Chan, Nature (London) **427**, 225 (2004); Science **305**, 1941 (2004).
 - [17] S. Sasaki, R. Ishiguro, F. Caupin, H. J. Maris, and S. Balibar, Science, **313**, 1098 (2006).
 - [18] L. Pollet, M. Boninsegni, A. B. Kuklov, N. V. Prokof'ev, B. V. Svistunov, and M. Troyer, Phys. Rev. Lett. **98**, 135301 (2007).
 - [19] P. Sengupta, L. P. Pryadko, F. Alet, M. Troyer, and G. Schmid, Phys. Rev. Lett. **94**, 207202 (2005); S. Wessel and M. Troyer, Phys. Rev. Lett. **95**, 127205 (2005).
 - [20] G. G. Batrouni and R. T. Scalettar, Phys. Rev. Lett. **84**, 1599 (2000).

- [21] J. Steinhauer, R. Ozeri, N. Katz, and N. Davidson, Phys. Rev. Lett. **88**, 120407 (2002).
- [22] P. T. Ernst, S. Götze, J. S. Krauser, K. Pyka, D.-S. Lühmann, D. Pfannkuche, and K. Sengstock, Nat. Phys. **6**, 56 (2009).
- [23] M. Greiner, O. Mandel, T. Esslinger, T. W. Hänsch, and I. Bloch, Nature (London) **415**, 39 (2002).
- [24] L. P. Pitaevskii and S. Stringari, *Bose-Einstein Condensation* (Oxford Science Publications, Oxford, 2003).
- [25] Recent theoretical work has proposed a way to measure the superfluid fraction in cold atom experiments with the use of a synthetic vector potential for atoms [26], but no experiment has tried it yet.
- [26] N. R. Cooper and Z. Hadzibabic, Phys. Rev. Lett. **104**, 030401 (2010).
- [27] L. De Sarlo, L. Fallani, J. E. Lye, M. Modugno, R. Saers, C. Fort, and M. Inguscio, Phys. Rev. A **72**, 013603 (2005).
- [28] J. Mun, P. Medley, G. K. Campbell, L. G. Marcassa, D. E. Pritchard, and W. Ketterle, Phys. Rev. Lett. **99**, 150604 (2007).
- [29] D. E. Miller, J. K. Chin, C. A. Stan, Y. Liu, W. Setiawan, C. Sanner, and W. Ketterle, Phys. Rev. Lett. **99**, 070402 (2007).
- [30] M. Vengalattore, J. Guzman, S. R. Leslie, F. Serwane, and D. M. Stamper-Kurn, Phys. Rev. A **81**, 053612 (2010).
- [31] K. Baumann, C. Guerlin, F. Brennecke, and T. Esslinger, Nature (London) **464**, 1301 (2010).
- [32] R. T. Scalettar, G. G. Batrouni, A. P. Kampf, and G. T. Zimanyi, Phys. Rev. B **51**, 8467 (1995).
- [33] D. Yamamoto and I. Danshita, in preparation.
- [34] H. Matsuda and T. Tsuneto, Suppl. Prog. Theor. Phys. **46**, 411 (1970).
- [35] C. Pich and E. Frey Phys. Rev. B **57**, 13712 (1998).
- [36] C. Menotti, C. Trefzger, and M. Lewenstein, Phys. Rev. Lett. **98**, 235301 (2007).
- [37] A. Smerzi, A. Trombettoni, P. G. Kevrekidis, and A. R. Bishop, Phys. Rev. Lett. **89**, 170402 (2002).
- [38] C. Menotti, A. Smerzi, and A. Trombettoni, New J. Phys. **5**, 112 (2003).
- [39] E. Zhao and A. Paramekanti, Phys. Rev. Lett. **96**, 105303 (2006).
- [40] A. A. Burkov and A. Paramekanti, Phys. Rev. Lett. **100**, 255301 (2008).
- [41] R. Ganesh, A. Paramekanti, and A. A. Burkov, Phys. Rev. A **80**, 043612 (2009).
- [42] Y. Yunomae, D. Yamamoto, I. Danshita, N. Yokoshi, and S. Tsuchiya, Phys. Rev. A **80**, 063627 (2009).
- [43] S. Konabe and T. Nikuni, J. Phys. B **39**, S101 (2006); J. Low Temp. Phys. **150**, 12 (2008).
- [44] K. Iigaya, S. Konabe, I. Danshita, and T. Nikuni, Phys. Rev. A **74**, 053611 (2006).
- [45] M. Kunimi, Y. Nagai, and Y. Kato, e-print arXiv:1005.3936.